Materials Chemistry and Physics 114 (2009) 595–598

Contents lists available at ScienceDirect

Materials Chemistry and Physics

journal homepage: www.elsevier.com/locate/matchemphys

Corrosion behaviors of austenitic Fe–30Mn–7Al–*x*Cr–1C alloys in 3.5% NaCl solution

Y.H. Tuan, C.S. Wang, C.Y. Tsai, C.G. Chao, T.F. Liu *

Department of Materials Science and Engineering, National Chiao Tung University, 1001 Ta Hsueh Road, Hsinchu 30049, Taiwan

ARTICLE INFO

Article history:
Received 28 May 2008
Received in revised form
18 September 2008
Accepted 2 October 2008

Keywords:
Alloy
Corrosion
Electrochemical techniques
Carbides

ABSTRACT

The corrosion behaviors of the as-quenched Fe–30 wt.%Mn–7 wt.%Al–*x* wt.%Cr–1 wt.%C alloys (*x* = 0, 3, 6 and 9) in 3.5% NaCl have been investigated. Passivation could be observed for all the alloys except for the alloy without Cr content. The corrosion potential (E_{corr}) and pitting potential (E_{pp}) increased pronouncedly with increasing Cr content up to 6 wt.%, and decreased as Cr content up to 9 wt.%. The decrease of E_{corr} and E_{pp} of the alloy containing 9 wt.% Cr was due to the formation of $(Fe,Mn,Cr)_7C_3$ carbides in the austenite matrix and on the grain boundaries. It is noted that the corrosion behaviors of the austenitic Fe–Mn–Al–Cr–C alloys with higher Cr (≥3 wt.%) content have never been reported in previous literatures.

1. Introduction

The austenitic Fe–Mn–Al–C quaternary alloys have many advantages, such as low cost, low density, high strength, high toughness, and good oxidation resistance [1–6]. However, the corrosion resistance of the austenitic Fe–Mn–Al–C alloys in aqueous environments was not adequate for applications in industry [5–13]. Therefore, many researchers tried to improve the corrosion resistance of the austenitic Fe–Mn–Al–C alloys by adding chromium and decreasing carbon content [6,9,14–17]. Since Cr and C are ferrite and austenite formers in ferrous alloys, respectively, the Fe–Mn–Al–Cr–C alloys with higher Cr and lower C contents consist of (austenite + ferrite) dual-phases. Some literatures showed that Fe–(21.5–27.7) wt.%Mn–(8.9–9.9) wt.%Al–(3.1–6.2) wt.%Cr–(0.33–0.42) wt.%C alloys exhibited austenite and ferrite dual-phases, and the mechanical properties of the dual-phase Fe–Mn–Al–Cr–C alloys were far inferior to those of austenitic ones. In order to obtain full austenitic structure, a proper combination of chromium and carbon contents was treated. In the previous studies [5,6], it was reported that the Fe–(29.5–31.3) wt.%Mn–(8.4–8.9) wt.%Al–(2.6–2.8) wt.%Cr–(0.98–1.06) wt.%C alloys had a single-phase austenite, and the corrosion resistance of the austenitic Fe–Mn–Al–Cr–C alloys was indeed superior to that of the austenitic Fe–Mn–Al–C or dual-phase Fe–Mn–Al–Cr–C alloys. However, to date, information concerning the corrosion behaviors of the austenitic Fe–Mn–Al–Cr–C alloys with higher Cr (≥3 wt.%) content is very deficient. In this study, the electrochemical corrosion properties of four austenitic Fe–30 wt.%Mn–7 wt.%Al–1 wt.%C alloys with 0, 3, 6 and 9 wt.% Cr contents in 3.5% NaCl solution were investigated to evaluate the effects of Cr content on the corrosion resistance.

2. Experimental procedure

The chemical compositions of the alloys are shown in Table 1. The alloys were prepared by melting commercial pure Fe, Mn, Al, Cr and carbon powder in an induction furnace under a controlled protective argon atmosphere. The melt was cast into 30 mm × 50 mm × 200 mm ceramic shell mold. After being homogenized at 1473 K for 24 h, the ingots were sectioned into 12 mm × 12 mm × 5 mm slices. These slices were subsequently solution heat-treated in vacuum furnace at 1373 K for 2 h and then rapidly quenched into room-temperature water. Potentiodynamic polarization curves were measured in 3.5% NaCl solution at 298 K. Electrochemical polarization curves were obtained by using an EG&G Princeton Applied Research Model 273 galvanostat/potentiostat. Specimens with an exposed surface area of ~1 cm^2 were ground with 2000-grit SiC paper and then with 1.5 μm Al_2O_3 powder, washed in distilled water and rinsed in acetone prior to passivation. Potentiodynamic polarization curves were obtained at a potential scan rate of 5 mV s^{-1} from −1 to 0.5 V. The concentration of elements in the passive film was examined by Auger electron spectroscopy (AES) and X-ray photoelectron spectroscopy (XPS). As well known, the composition quantification of AES is very poor due to matrix effect, peaks overlapping and surface roughness, etc. However, the depth profiling is one of the most important and convenient application of AES for analyzing the composition of thin surface layer. Therefore, the depth profiling of AES is an appropriate and effective method for analyzing the composition distributions of the passive film in this experiment [18,19]. Microstructures were examined by using optical microscopy and transmission electron microscopy (TEM). TEM specimens were prepared by means of a double-jet electropolisher with an electrolyte of 15% perchloric acid, 25% acetic

* Corresponding author. Tel.: +886 3 5131288; fax: +886 3 5713987.
E-mail addresses: tfliu@cc.nctu.edu.tw, yixduan@gmail.com, phyxsiusmilo@gmail.com (T.F. Liu).

0254-0584/$ – see front matter © 2008 Elsevier B.V. All rights reserved.
doi:10.1016/j.matchemphys.2008.10.009

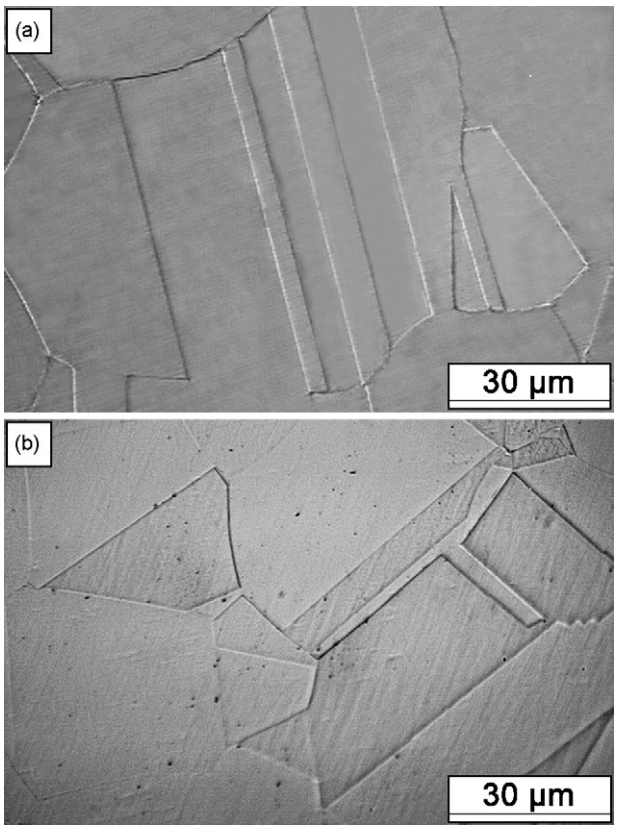

Fig. 1. Optical micrographs of the Fe–30 wt.%Mn–7 wt.%Al–(6, 9) wt.%Cr–1 wt.%C alloys. (a) 6 wt.%Cr, and (b) 9 wt.%Cr.

Table 1
Chemical compositions of the present alloys (wt.%).

Alloy	Mn	Al	Cr	C	Fe
A(0Cr)	29.18	7.05	0	0.96	Bal.
B(3Cr)	29.92	7.12	3.01	1.04	Bal.
C(6Cr)	30.12	7.06	5.96	1.01	Bal.
D(9Cr)	30.02	7.08	9.05	0.98	Bal.

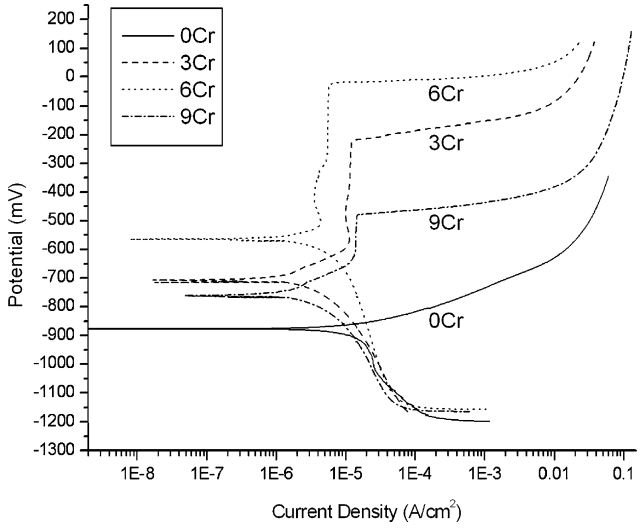

Fig. 2. Potentiodynamic polarization curves for the five Fe–30 wt.%Mn–7 wt.%Al–(0, 3, 6, and 9) wt.%Cr–1 wt.%C alloys in 3.5% NaCl solution.

Table 2
The electrochemical parameters from potentiodynamic polarization curves for the Fe–30 wt.%Mn–7 wt.%Al–(0, 3, 6 and 9) wt.%Cr–1 wt.%C alloys in 3.5% NaCl solution.

Alloy	Electrochemical parameters from polarization curves			
	E_{corr} (mV)	E_{cr} (mV)	E_{pp} (mV)	Ip (A cm^{-2})
A(0Cr)	−877	–	–	–
B(3Cr)	−712	−588	−224	4.1E−05
C(6Cr)	−556	−518	−27	5.75E−06
D(9Cr)	−754	−599	−472	1.78E−05

E_{corr}, corrosion potential; E_{cr}, critical potential for active–passive transition; E_{pp}, pitting potential; Ip, passive current density, minimum value.

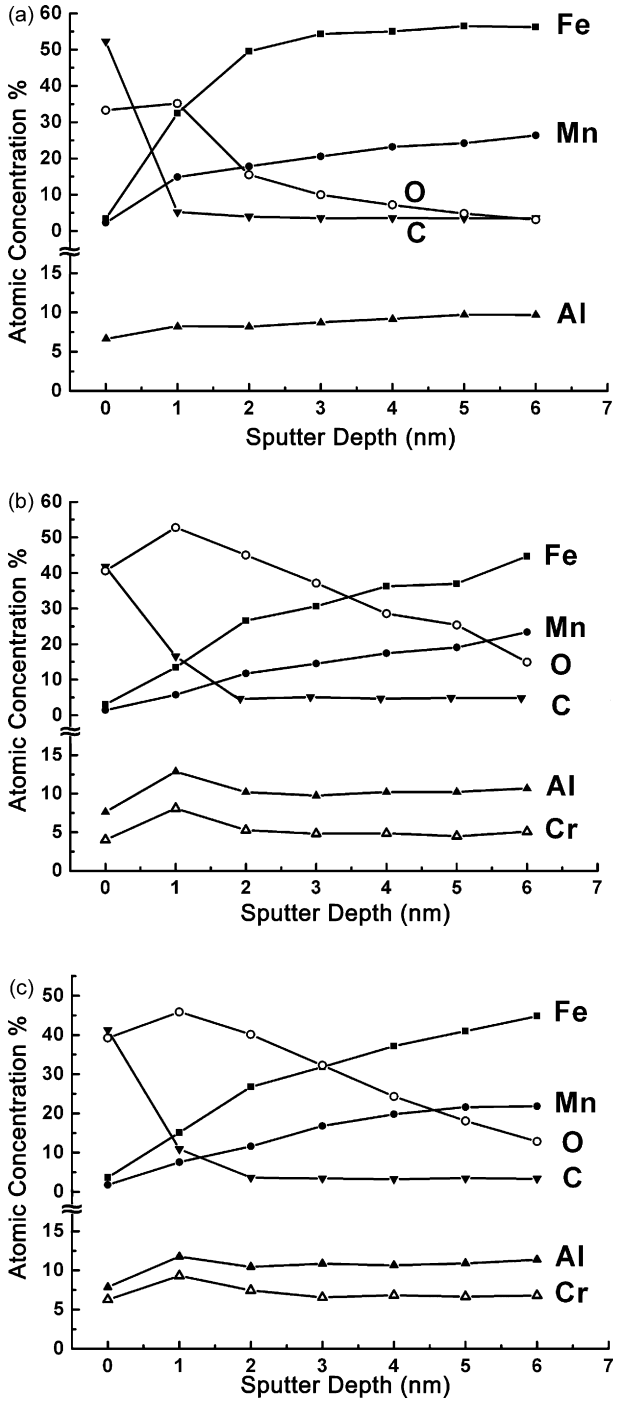

Fig. 3. AES depth profiles for the passive film of the Fe–30 wt.%Mn–7 wt.%Al–(0, 6, and 9) wt.%Cr–1 wt.%C alloys. (a) 0 wt.%Cr, (b) 6 wt.%Cr, and (c) 9 wt.%Cr.

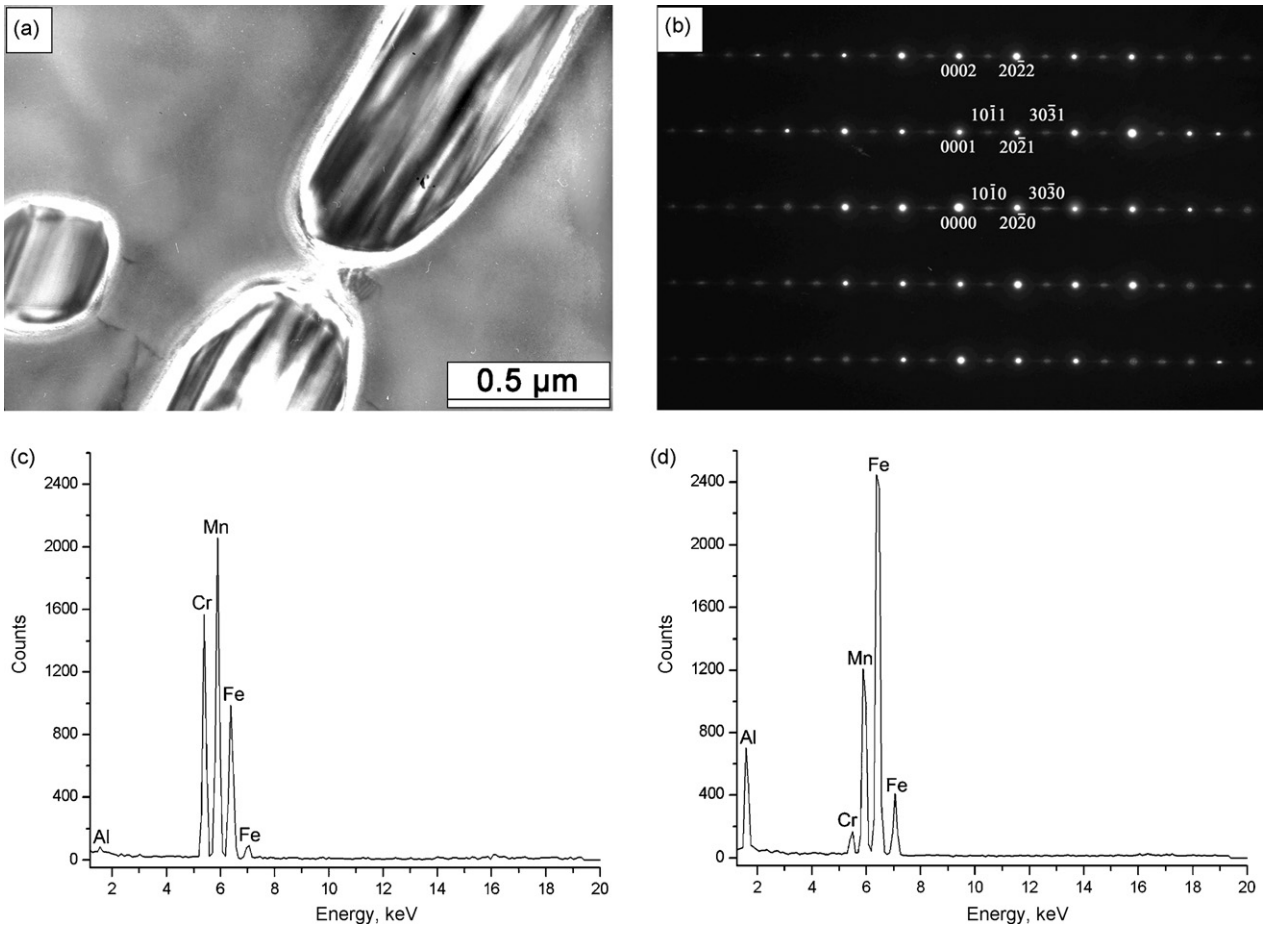

Fig. 4. Transmission electron micrographs of the Fe–30 wt.%Mn–7 wt.%Al–9 wt.%Cr–1 wt.%C alloy. (a) BF, and (b) a selected-area diffraction pattern taken from a $(Fe,Mn,Cr)_7C_3$ carbide in (a). The zone axis of the $(Fe,Mn,Cr)_7C_3$ carbide is $[2\,\bar{1}\,\bar{1}\,0]$ (c) and (d) two typical EDS profiles obtained from the $(Fe,Mn,Cr)_7C_3$ carbide and the austenite matrix nearby the $(Fe,Mn,Cr)_7C_3$ carbide, respectively.

acid and 60% ethanol. Electron microscopy was performed on JEOL-2000FX STEM operating at 200 kV. This microscope was equipped with a Link ISIS 300 energy-dispersive X-ray spectrometer (EDS) for chemical analysis. Quantitative analyses of elemental concentrations for Fe, Mn, Al and Cr were made using the Cliff-Lorimer ratio thin section method.

3. Results and discussion

Optical microscopy examinations showed that the as-quenched microstructure of the alloys A(0Cr) through C(6Cr) was single-phase austenite. Fig. 1(a) shows a typical optical micrograph of the alloy C(6Cr), indicating single-phase austenite with annealing twins. Transmission electron microscopy examinations indicated that besides the austenite phase, no evidence of carbides could be detected in the as-quenched alloys A(0Cr) through C(6Cr). Fig. 1(b) is an optical micrograph of the alloy D(9Cr), revealing the presence of some carbides in the austenite matrix and on the grain boundaries. It seems to imply that Cr could be completely dissolved in the austenite matrix at 1373 K as Cr $\leq$6 wt.%, and carbides could be formed at this temperature as Cr up to 9 wt.%. Potentiodynamic polarization curves for the four Fe–Mn–Al–Cr–C alloys in 3.5% NaCl solution are shown in Fig. 2. The electrochemical parameters are summarized in Table 2. E_{corr} of the alloys with different Cr content was varied from −556 to −877 mV. Alloy C(6Cr) has the noblest E_{corr} (−556 mV). Similarly, with increasing Cr content from 3 to 6 wt.%, the E_{pp} was drastically increased from −224 to −27 mV. However, with further increasing the Cr content to 9 wt.%, E_{pp} became more negative (−472 mV). The results indicate that the alloy C(6Cr) had the highest resistivity to pitting damage. Passivation could be observed for all the alloys except for the alloy without Cr content. In Fig. 2, it is clearly seen that the passive region increased as Cr content increased from 0 to 6 wt.%, and decreased as Cr content up to 9 wt.%. In order to determine the chemical composition and the valence state of element in passive film formed on the alloys in 3.5% NaCl solution, the technique of AES/XPS was undertaken. Fig. 3 indicates that the depth-concentration profiles for passive film formed on the alloys A(0Cr), C(6Cr) and D(9Cr). The detection of carbon concentration of outmost layer may be due to surface contamination. The O concentration of the alloy A(0Cr) was much smaller than that of the alloys C(6Cr) and D(9Cr) in depth profile. In Fig. 3(a), it is clear that passive film was not obvious in the alloy without Cr content. However, in the alloys C(6Cr) and D(9Cr), the O concentration at the surface was much higher than that in the matrix, as illustrated in Fig. 3(b) and (c). The Mn and Fe contents in the outmost surface were much lower than those in the matrix, but Cr and Al contents were reverse tendency. It means that the Cr and Al enrichment was attributed to the preferential dissolution of unstable oxides of Fe and Mn into electrolyte solution, and then replacement by Cr and Al within the oxide layer. There were broad peaks of Cr and Al at a depth of 0–2 nm, which corresponded with the peak of O. This implies that the increase of Cr and Al in oxides is likely to be responsible for the improved stability of the passive film. However, the AES analysis for passive film cannot explain the reason why the E_{corr} of the alloy D(9Cr) decreased

(more negative), as indicated in Table 2. In order to obtain more information, the alloy with 9 wt.% Cr content was examined by TEM. Fig. 4(a), a bright-field electron micrograph, clearly reveals the presence of carbides in the austenite matrix. Fig. 4(b) is a selected-area diffraction pattern taken from a carbide. Compared to the previous studies [20], it is clear that the carbide is $(Fe,Mn,Cr)_7C_3$ with lattice parameters $a = 1.398$ nm and $c = 0.452$ nm. Fig. 4(c) and (d) are two EDS profiles taken from a $(Fe,Mn,Cr)_7C_3$ carbide and the austenite matrix nearby the $(Fe,Mn,Cr)_7C_3$ carbide, respectively. The quantitative analyses of ten different EDS profiles showed that the chemical composition of the carbide was Fe–0.56 wt.%Al–40.12 wt.%Mn–34.39 wt.%Cr (EDS with the thick-window detector can only detect the elements with atomic number 11 or above, hence carbon is unable to be examined by this method), and the chemical composition of the austenite matrix nearby the carbide was Fe–10.51 wt.%Al–25.48 wt.%Mn–2.73 wt.%Cr. It is clearly seen that the Cr content in the $(Fe,Mn,Cr)_7C_3$ carbide is up to 34.39 wt.%, which is much higher than that in the austenite matrix nearby the $(Fe,Mn,Cr)_7C_3$ carbide. It is thus expected that the conspicuous decrease of the Cr content in the austenite matrix was ascribed to the formation of Cr-rich $(Fe,Mn,Cr)_7C_3$ carbides. Therefore, it is deduced that the formation of Cr-rich $(Fe,Mn,Cr)_7C_3$ carbides would lead to the decrease of E_{corr} and E_{pp} of the alloy D(9Cr).

Based on the preceding results, it is clear that no evidence of passivation could be found in the alloy A(0Cr) and the E_{corr} of the alloy was −877 mV. This result is similar to that examined by other workers in the as-quenched austenitic Fe–(26.0–32.2) wt.%Mn–(8.3–10.0) wt.%Al–(0.85–1.45) wt.%C alloys in 3.5% NaCl solution, in which they reported that only narrow passive region could be observed and the E_{corr} of the alloys was in the range from −789 to −920 mV [5–9,14]. However, an obvious broad passive region could be detected in the present alloys containing Cr. This shows that the Cr addition is indeed beneficial for the corrosion resistance of the austenitic Fe–Mn–Al–C alloys in NaCl solution, which is in agreement with that examined by other workers in the austenitic Fe–(29.5–31.3) wt.%Mn–(8.4–8.9) wt.%Al––(2.6–2.8) wt.%Cr–(0.98–1.06)wt.%C alloys [5,6]. In addition, the E_{corr} value for the alloy B(3Cr) was −712 mV, which is comparable to about −720 mV for the as-quenched Fe–29.5 wt.%Mn–8.4 wt.%Al–2.6 wt.%Cr–1.06 wt.%C alloy in 3.5% NaCl solution reported by other workers [6]. In the present study, we have further shown that the 6.0 wt.% Cr addition was completely dissolved in the Fe–30 wt.%Mn–7 wt.%Al–1.0 wt.%C alloy at 1373 K. Thus, the E_{corr} and E_{pp} values would be pronouncedly increased to −556 and −27 mV, respectively, in the alloy C(6Cr). However, when the Cr addition was increased up to 9 wt.%, the Cr-rich $(Fe,Mn,Cr)_7C_3$ carbides could be detected in the as-quenched alloy D(9Cr). The formation of Cr-rich $(Fe,Mn,Cr)_7C_3$ carbides resulted in the drastic decrease of the E_{corr} and E_{pp} values.

4. Conclusions

The corrosion potential (E_{corr}) of the as-quenched Fe–30 wt.%Mn–7 wt.%Al–(0, 3, 6 and 9) wt.%Cr–1 wt.%C alloys increased from −877 to −556 mV as Cr content increased from 0 to 6 wt.%. However, the E_{corr} of the alloy with 9 wt.% Cr dropped to −754 mV due to the formation of $(Fe,Mn,Cr)_7C_3$ carbides in the austenitic matrix and on the grain boundaries. The result indicates that the alloy C (6Cr) exhibited the highest corrosion resistance in 3.5% NaCl solution. Passivation could be observed for all of the present alloys except for the alloy without Cr content.

Acknowledgements

The authors are pleased to acknowledge the financial support of this research by the National Science Council, Republic of China under Grant NSC95-2221-E-009-086-MY3.

References

[1] S.M. Zhu, S.C. Tjong, Metalls. Trans. A 29 (1998) 299.
[2] W.K. Choo, J.H. Kim, J.C. Yooh, Acta Mater. 45 (1997) 4877.
[3] I.S. Kalashnikov, O. Acselrad, L.C. Pereira, T. Kalichak, M.S. Khadyyev, J. Mater. Eng. Perform. 9 (2000) 334.
[4] S.C. Chang, Y.H. Hsiau, J. Mater. Sci. 24 (1989) 1117.
[5] S.C. Chang, J.Y. Liu, H.K. Juang, Corrosion. Eng. 51 (1995) 399.
[6] S.C. Chang, W.H. Weng, H.C. Chen, S.J. Lin, P.C.K. Chung, Wear 181–183 (1995) 511.
[7] W.T. Tsai, J.B. Duh, J.T. Lee, J. Mater. Sci. 22 (1987) 3517.
[8] J.B. Duh, W.T. Tsai, J.T. Lee, Corrosion November (1988) 810.
[9] M. Ruscak, T.P. Perng, Corrosion October (1995) 738.
[10] S.C. Tjong, C.S. Wu, Mater. Sci. Eng. 80 (1986) 203.
[11] S.C. Tjong, Surface Coat. Technol. 28 (1986) 181.
[12] C.J. Wang, Y.C. Chang, Mater. Chem. Phys. 76 (2002) 151.
[13] X.M. Zhu, Y.S. Zhang, Corrosion 54 (1998) 3.
[14] S.T. Shih, C.Y. Tai, T.P. Perng, Corrosion February (1993) 130.
[15] I.F. Tsu, T.P. Perng, Metall. Trans. A 22 (1991) 215.
[16] C.C. Wu, J.S. Chou, T.F. Liu, Metall. Trans. A 22 (1991) 2265.
[17] S.M. Zhu, S.C. Tjong, Scripta 36 (1997) 317.
[18] J.M. Walls, Methods of Surface Analysis, Cambridge University Press, New York, 1989.
[19] David Briggs, T. John, Grant (Eds.), Surface Analysis by Auger and X-Ray Photoelectron Spectroscopy, IM Publications, Chichester, 2003, p. 619.
[20] F. Ernst, Y. Cao, G.M. Michal, Acta Mater. 52 (2004) 1469.